THERMO-ELECTRO-MECHANICAL NUMERICAL MODELING WITH AN ANALYTICAL APPROXIMATION OF COUPLED THERMAL FATIGUE FAILURE PROCESS OF CORSET SAMPLES FROM SINGLE-CRYSTAL NICKEL-BASED SUPERALLOYS

A.V. Savikovskii[1*], A.S. Semenov[1], L.B. Getsov[2]

[1]SPBPU, Polytechnicheskaya 29, Russia

[2]NPO CKTI, Polytechnicheskaya 24, Russia

[*]temachess@yandex.ru

Abstract. The results of computations of the thermal and stress-strain state of single-crystal corset specimens subjected to the action of periodic electric current, leading to variable inhomogeneous heating and subsequent thermal fatigue failure, are presented. An analytic approximation was introduced for the process of nonstationary heating of corset sample and a comparation of modeling results with experimental data and analytic model was evaluated which showed a good correlation with experimental data. The influence of maximum value and range of temperature and also influence of a delay time at the maximum temperature on the number of cycles before the macrocrack formation were investigated. Also an analytic approximation was considered of a delay influence and comparison of the computational results and analytic formulaes with the experimental data for various single-crystal nickel-based superalloys showed a good accuracy.

1. Introduction

Single-crystal nickel based superalloys [1] are used for production of gas turbine engines (GTE). These materials have a pronounced anisotropy of properties and a dependence properties on temperature and thermal fatigue strength of superalloys is not studied very well. For the investigation of thermal fatigue durability under a wide range of temperatures with and without intermediate delays the experiments are carried out on different types of samples, including corset (plane) specimen on the installation developed in NPO CKTI [2] (see Fig. 1). Fixed in axial direction by means of two bolts with a massive foundation the corset sample (see Fig. 2) is heated periodically by passing electric current through it. During cycling the maximum and minimum temperatures are automatically maintained constant.

Fig. 1. Installation for carrying out experiments on thermal fatigue.

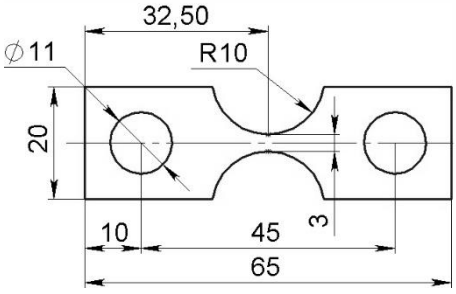

Fig. 2. Geometry corset sample for thermal fatigue experiment.

The aim of the study is to investigate numerically a process of heating and cooling of corset sample and to request analytical approximation for this process, to study numerically the stress-strain state of the sample during cyclic heating and cooling due to its clamping and to study systematically the effect of delay at maximum temperature on the thermal fatigue durability on the base of the deformation criterion [3-5] of thermal-fatigue failure for single crystal superalloys using the results of finite element (FE) simulation of full-scale experiments and results of analytical formulaes. The

results of simulation and their verification are obtained for the different single-crystal nickel-based superalloys: VZhM4, VIN3 and ZhS32.

2. Results of numerical thermo-electric nonstationary analysis and analytical approximation for temperature changing during time

Modeling of a heating process by an electric current and a cooling process without an electric current of the corset sample was carried in the FE program ANSYS with taking into account the temperature dependence of all material properties, thermoelectric contacts between the sample and an equipment, nonstationary Joule heating, the convective heat exchange and radiative heat transfer between the sample and the environment. The full-scale FE model of experimentation object including discrete models of the specimen and the setup is presented in Fig. 3.

The problem was solved for different single-crystal nickel-based superalloys VZhM4, VIN3 and ZhS32. The properties of three alloys were accepted the same because of lack of information about nickel alloys' properties dependence on temperature.

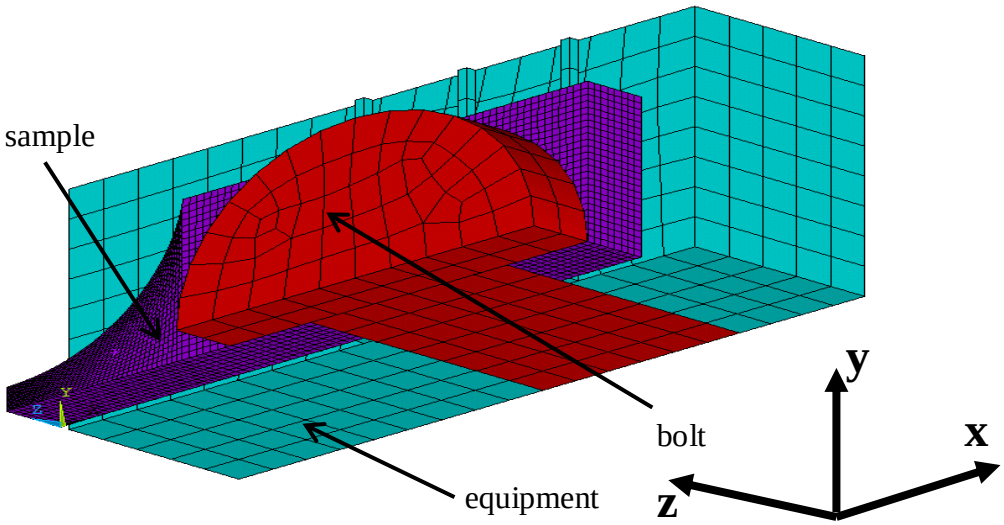

Fig. 3. Finite-element model in thermoelectric problem.

Modeling of heating and cooling processes of sample was carried out for five temperature regimes (modes): 100÷800, 150÷900, 250÷1000, 500÷1050 and 700÷1050 °C. There are nonstationary experimental data for four regimes: 100÷800 °C, a heating time is 19s, a cooling time is 46s, 150÷900 °C, a heating time is 42s, a cooling time is 59,5s, 500÷1050 °C, a heating time is 14s, a cooling time is 10s, 700÷1050 °C, a heating time is 8s, a cooling time is 7s. In case of temperature mode 250÷1000 time of heating is 80 s. The used in FE simulations material properties for the single crystal nickel superalloy sample and for the steel equipment were taken from literature [6], [7]-[9] (see also Tables 1-2). While specifying the properties of nickel alloy and steel the implementation of the Wiedemann-Franz's law was controlled: $\lambda \cdot \rho_e = LT$, where λ is the thermal conductivity, ρ_e is the specific electrical resistance, T is the temperature in K, L= 2.22 *10^{-8} W·Ω·K^{-2} is the Lorentz's constant.

Table 1 Thermo-electric properties of nickel superalloy used in simulations:

T	°C	20	200	400	600	800	1000	1150	Ref.
ρ	Kg/m^3	8550	8500	8450	8400	8350	8330	8310	[7]
C_p	J/(kg·K)	440	520	520	540	570	590	600	[7]
λ	W/(m·K)	7.4	11.2	14.1	16.3	19.8	26.7	36.7	[6]
ρ_e	Ω·m	$8.7\cdot10^{-7}$	$9.3\cdot10^{-7}$	$1\cdot10^{-6}$	$1.2\cdot10^{-6}$	$1.2\cdot10^{-6}$	$1\cdot10^{-6}$	$8.9\cdot10^{-7}$	[6]

Table 2 Thermo-electric properties of pearlitic steel used in simulations:

T	$^{\circ}C$	**27**	**127**	**327**	**527**	**927**	**1127**	Ref.
ρ	Kg/m^3	7778	7772	7767	7762	7754	7751	[8]
C_p	J/(kg·*K*)	469	506	521	660	577	530	[8]
λ	W/(m·*K*)	48	47	41	37	23	12	[8]
ρ_e	Ω·m	$2\cdot10^{-7}$	$2.6\cdot10^{-7}$	$4.2\cdot10^{-7}$	$6.4\cdot10^{-7}$	$1.16\cdot10^{-6}$	$1.4\cdot10^{-6}$	[9]

The coupled three-dimensional transient thermo-electrical analysis has been performed. Due to the symmetry in respect to the *xz* and *yz* planes, a quarter of the structure was considered. The thermal and electric contacts between the sample and bolts, between the sample and the foundation were taken into account. The initial temperature for the sample and the equipment was set to 30 °C. For the free surface of sample the boundary condition of convective heat transfer is used:

$$q_n = h(T - T_0)\ , \tag{1}$$

where n is the normal to body, q_n is the heat flux density, $h = 20\frac{W}{m^2K}$ is the coefficient of convective heat transfer, T_0 is the ambient temperature.

The condition of radiative heat transfer was also set on the surfaces of central (high temperature) part of the sample (10 mm length):

$$q_n = \varepsilon\sigma_{SB}(T^4 - T_0^4)\ , \tag{2}$$

where ε = 0.8 is the black factor of the body, $\sigma_{SB} = 5.67\cdot10^{-8}Wm^{-2}K^{-4}$ is the coefficient of Stefan-Boltzmann.

In order to realize an analytical approximation for the curve of temperature change in time, we consider the problem of mathematical physics of heating the sample with a constant cross-section. For example, the sample has a length and a depth the same with the corset sample 32.5 mm and 3 mm respectively, but the sample with a constant cross section has width is equal to 10 mm (fig. 4).

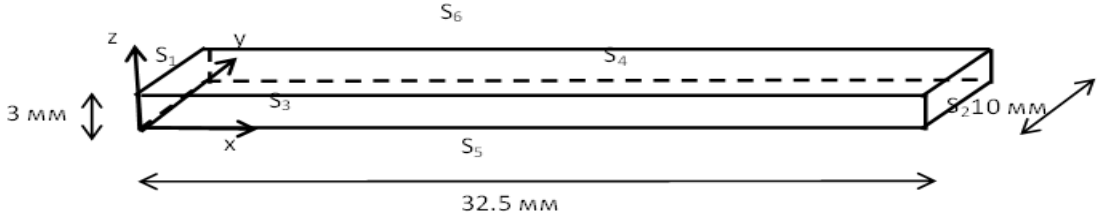

Fig. 4. The statement of simplify thermal problem

The aim of our analogy is to simplify a task of heating the corset sample to one-dimensional problem with equivalent boundary conditions. The boundary conditions of a lack of heat flow were set on surfaces S_3, S_4, S_5, S_6. On the surface S_2 was fixed the temperature, on the surface S_1 boundary condition of convection with a convective heat transfer coefficient h is equal to $20\frac{W}{m^2K}$. The sample in the thermal problem is heating by electric current that's why boundary condition of heat generation was set on the sample is equal to some constant Q, which does not depend on time.

The equation of unsteady thermal conductivity can be represented as

$$\Delta T - \frac{\partial T}{\partial \tau} = -\frac{Q}{\lambda}\ [10], \tag{3}$$

where T is the temperature, Δ *i*s the laplassian operator, τ is the slow time and $\tau = \frac{\lambda t}{C_\rho \rho}$, Q is the heat generation, λ, C_ρ, ρ are the conductive coefficient, the specific heat and the density respectively. Considering that boundary conditions in the axis y and z are a lack of heat flux and overwriting the laplassian operator in Cartesian coordinates, we come to the equation

$$\frac{d^2T}{dx^2} - \frac{\partial T}{\partial \tau} = -\frac{Q}{\lambda}, \tag{4}$$

where x is the axial coordinate along the sample. Representing T as a sum of two functions $T_1(x)$ and $T_2(x, \tau)$, we come to two equations. One of these equations has two variable, x and time:

$$\frac{\partial^2 T_2}{\partial x^2} - \frac{\partial T_2}{\partial \tau} = 0 \tag{5}$$

Using Fourier method [10], we put two equations with variables X and $\boldsymbol{\Omega}$ respectively. The equation with a variable X is $X'' + \beta X = 0,$ (6)
where β is the arbitrary constant. Boundary conditions for the equation (6) are a convective boundary condition in the middle of the sample and temperature is equal to zero on the edges. Also the equation with a variable $\boldsymbol{\Omega}$ is $\Omega' + \beta\Omega = 0,$ (7)
where β is the arbitrary constant from equation (6). Finding a solution of equation (6) as a sum of sinus and cosine with constants and substituting boundary conditions we put a transcendental equation: $\mathrm{tg}\gamma_n = -\frac{\lambda\gamma_n}{hl}$, (8)
where $\gamma_n = \sqrt{\beta_n}$l, h = $20\frac{W}{m^2K}$,l = 32.5 mm. General solution of equation (7) is $\Omega = Ce^{-\beta_n\tau}$, where β_n is the eigenvalue and $\beta_n = \frac{\gamma_n{}^2}{l^2}$. In general, we put solution $T_2(x, \tau) = C\cdot X(x)\cdot e^{-\frac{\gamma_n{}^2}{l^2}\tau}$, where γ_n *can* be found from an equation (8). We use simple approximation for temperature changing in time for a heating and cooling as one exponential with exponent - $\frac{\gamma_n{}^2}{l^2}$ with constants. Returning to usual time t, we can rewrite an analytical approximation for heating as:

$$T = A - B\cdot e^{-\frac{\gamma_n{}^2}{l^2}\cdot\frac{\lambda}{C_\rho\rho}t}, \quad (9)$$

where A and B are constants, which are selected from conditions of equality in the beginning of the heating to minimum temperature in the cycle and in the end of the heating to maximum temperature in the cycle, γ_n *can* be found from a transcendental equation (8), l is the length of the sample. For a process of the cooling of the sample similar analytical approximation was considered:

$$T = C + D\cdot e^{-\frac{\gamma_n{}^2}{l^2}\cdot\frac{\lambda}{C_\rho\rho}t}, \quad (10)$$

Materials constants λ, C_ρ , ρ were set to $20\frac{W}{m^2K}$, $550\frac{J}{kg\cdot K}$ and 8400 $\frac{Kg}{m^3}$ respectively.Comparison of experimental data, computational results and analytical approximation for temperature changing in time are presented in fig. 5 for temperature modes 100÷800, 150÷900, 500÷1050 and 700÷1050 °C.

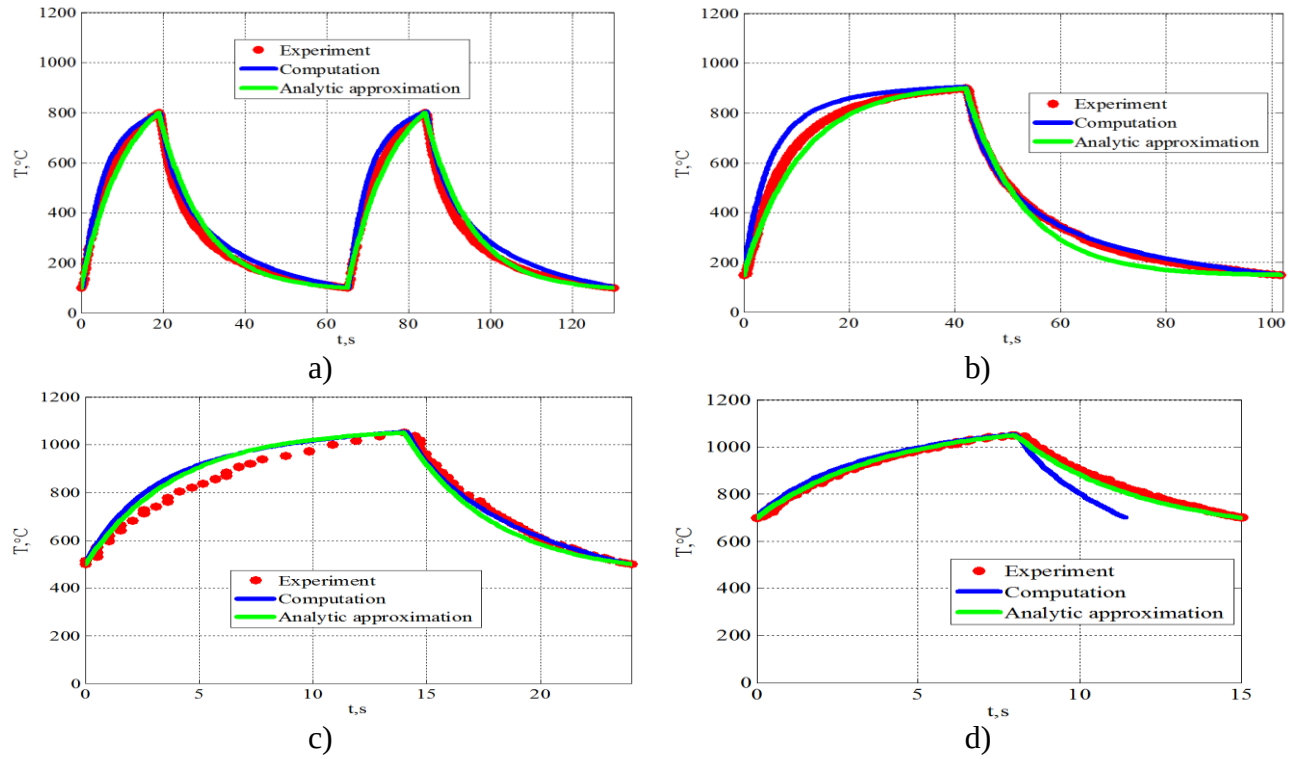

Fig. 5. Comparison of experimental data, simulation results and analytical approximation for temperature modes: a) 100÷800, a heating time is 19s, a cooling time is 46s, b) 150÷900 °C, a heating time is 42s, a cooling time is 59,5s, c) 500÷1050 °C, a heating time is 14s, a cooling time is 10s, d) 700÷1050 °C, a heating time is 8s, a cooling time is 7s.

Comparison of experimental data and computations for maximum temperature and temperature distributions along the corset sample in different times for temperature modes 150÷900, 250÷1000, 500÷1050 and 700÷1050 °C are shown in fig. 6.

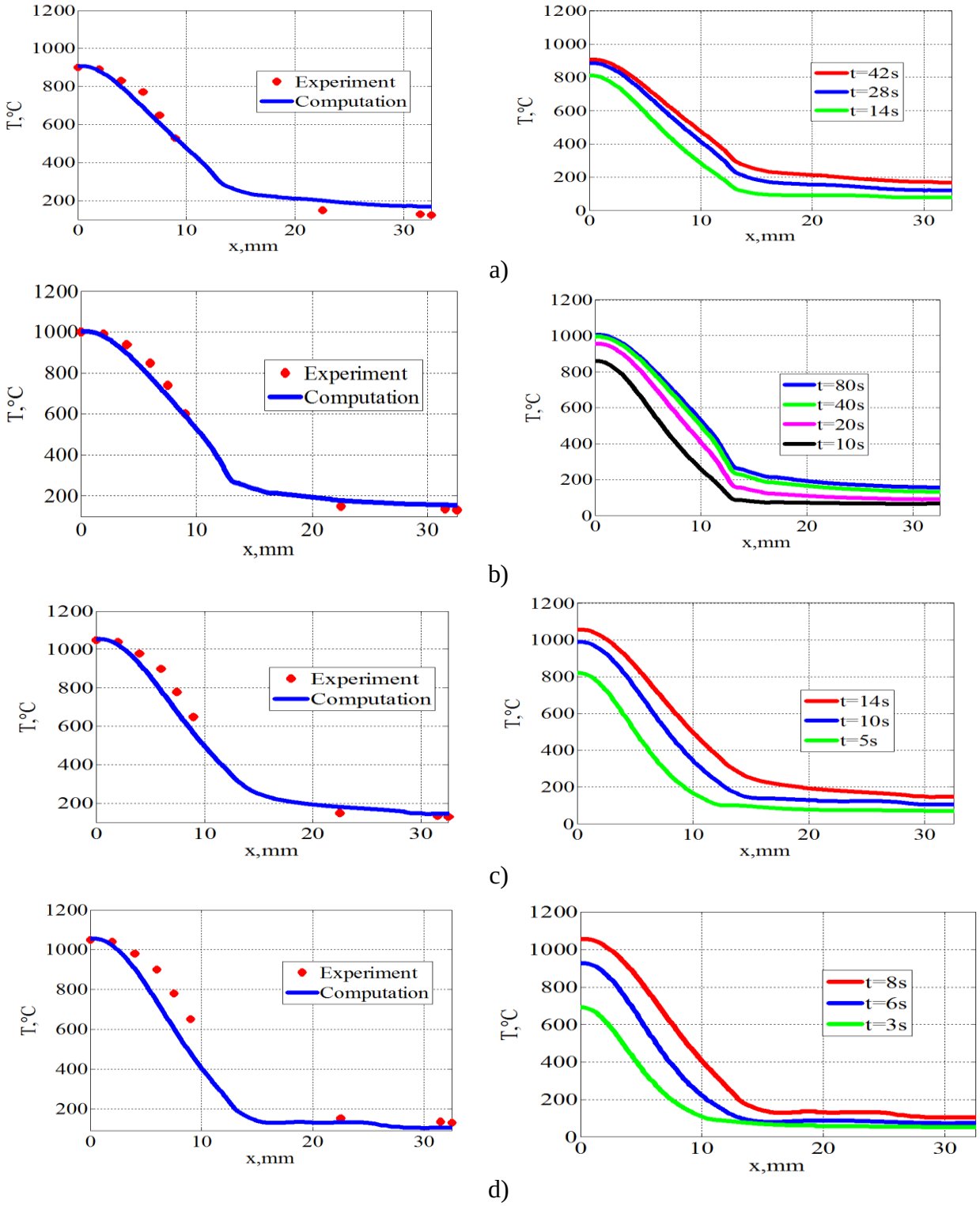

Fig.6. Comparison of experimental data and computations for maximum temperature and temperature distributions along the corset sample in different times for temperature modes a) 150÷900, a heating time is 42s, b) 250÷1000, a heating time is 80s c) 500÷1050, a heating time is 14s d) 700÷1050 a heating time is 8s

Temperature plane distributions for maximum temperature for temperature modes 100÷800, 150÷900, 250÷1000 and 700÷1050 °C are presented in fig. 7.

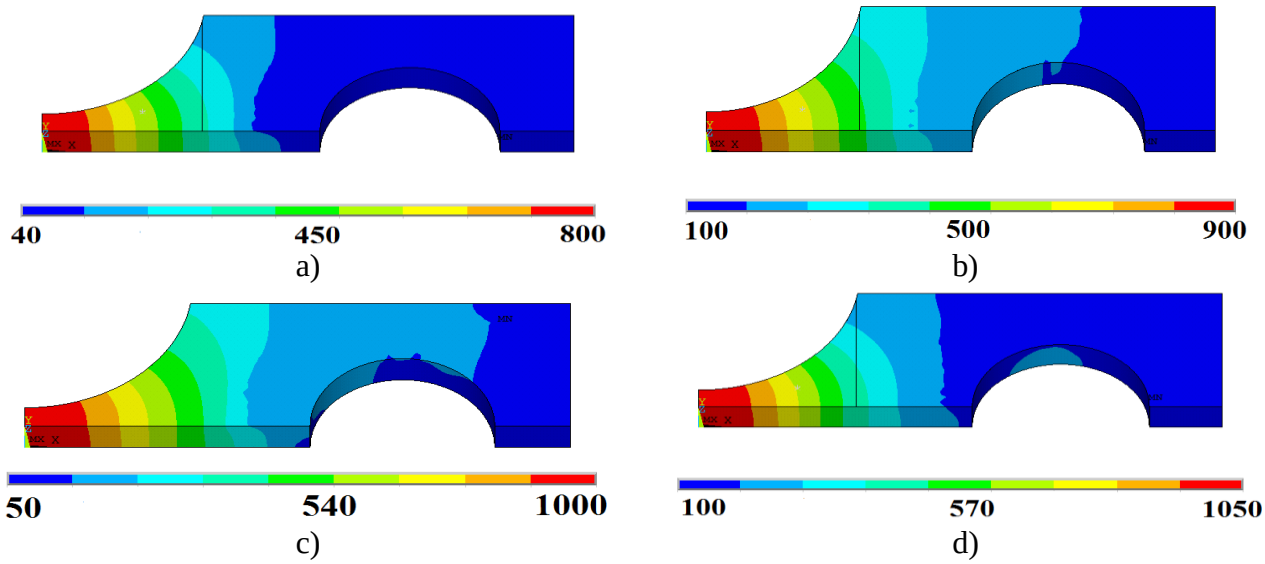

Fig.7. Temperature plane distributions for maximum temperature for temperature modes a) 100÷800, b) 150÷900, c) 250÷1000 d) 500÷1050 °C

The obtained in thermo-electric problem the spatial and temporal distribution of the temperature field is the base for the strain and stress field computation within the framework of thermo-elasto-visco-plastic problem solution.

3. Results of thermo-elasto-visco-plastic analysis

The fixing of sample under heating leads to the high stress level and inelastic strain appearance. The local strain and stress concentration is observed in the central (working) part of sample. The FE simulation is required for the computation of inhomogeneous stress and inelastic strain fields. Modeling of inelastic deformation in the corset samples has been performed with taking into account of the temperature dependence of all material properties, anisotropy of mechanical properties of single crystal sample, kinematic and isotropic hardening, inhomogeneous nonstationary temperature field, mechanical contacts between bolt and the specimen, between specimen and foundation, friction between the contact surfaces, temperature expansion in the specimen and foundation. The viscous properties were taking into account because of a quick time of heating and cooling of the corset sample.

The two FE formulations for the thermomechanical problem have been considered:

- with taking into account equipment;
- without taking into account equipment (simplified formulation [11] for the sample only).

Using of the second formulation provides significant saving computational time due to reduction in the number of degrees of freedom and refusal to solve a contact problem that is very actual for the numerous multivariant computations for different regimes of loading and the crystallographic orientations. One of the aims of the investigations was the selection of the equivalent (effective) length of the sample for the simplified formulation. The validity of the simplified formulation is based on the comparison with the results of full-scale formulation (with taking into account equipment), as well as on the comparison with the relative displacements of two markers measured in experiments.

In the general case there is no symmetry in the problem due to anisotropy of mechanical properties of single crystal sample. However in the important for practice case of [001] crystallographic orientation of sample the symmetry in respect to planes xz and yz (see Fig. 8) can be introduced. Equipment and bolts were modeled by linear elastic material (steel), and for the sample the elasto-visco–plastic model of the material was used. The problem was solved in a three-dimensional, quasi-static formulation. As boundary conditions the symmetry conditions were set: zero displacements on the y-axis on the xz plane and zero displacements on the x-axis

on the yz plane. On the lower side of the equipment zero displacements along the x and z axes were set. On the bolt cap the pressure of 100 MPa has been applied that is equivalent to the tightening force of the bolt. The temperature boundary conditions were set from the experimental data at maximum and minimum temperature with linear interpolation in time. The mechanical properties for the alloys VZHM4 and VIN3 were taken from the papers [12, 13] and for ZHS32 from [14] are presented in Table 3, 4, 5. The mechanical properties of bolts are taken for pearlitic steel [9].

Table 3. Mechanical properties of VZHM4 used in simulations [12]:

T	**^{0}C**	**20**	**700**	**800**	**900**	**1000**	**1050**
E_{001}	MPa	130000	101000	96000	91000	86000	82000
ν	-	0.39	0.42	0.422	0.425	0.428	0.43
α	1/K	$1.11\cdot10^{-5}$	$1.68\cdot10^{-5}$	$1.74\cdot10^{-5}$	$1.87\cdot10^{-5}$	$2.1\cdot10^{-5}$	$2.3\cdot10^{-5}$
σ_{Y001}	MPa	846	950	-	-	-	820
n	-	8	8	8	8	8	8
A	$MPa^{-n}s^{-1}$	$1\cdot10^{-42}$	$3\cdot10^{-31}$	$1\cdot10^{-29}$	$1\cdot10^{-28}$	$2\cdot10^{-27}$	$1\cdot10^{-26}$

Table 4. Mechanical properties of VIN3 used in simulations [13]:

T	**^{0}C**	**20**	**500**	**700**	**900**	**1000**	**1050**
E_{001}	MPa	126000	110000	104000	89000	80000	75000
ν	-	0.39	0.41	0.42	0.42	0.425	0.428
α	1/K	$1.21\cdot10^{-5}$	$1.33\cdot10^{-5}$	$1.4*10^{-5}$	$1.5\cdot10^{-5}$	$1.57\cdot10^{-5}$	$1.6\cdot10^{-5}$
σ_{Y001}	MPa	555	800	930	910	645	540
n	-	8	8	8	8	8	8
A	$MPa^{-n}s^{-1}$	$1\cdot10^{-42}$	$4\cdot10^{-34}$	$1.5\cdot10^{-30}$	$5.8\cdot10^{-27}$	$3.5\cdot10^{-25}$	$1.5\cdot10^{-24}$

Table 5. Mechanical properties of ZHS32 used in simulations [14]:

T	**^{0}C**	**20**	**700**	**800**	**900**	**1000**	**1050**
E_{001}	MPa	137000	110000	105000	99800	94800	92300
ν	-	0.395	0.4248	0.4284	0.4317	0.4347	0.4361
α	1/K	$1.24\cdot10^{-5}$	$1.6\cdot10^{-5}$	$1.7\cdot10^{-5}$	$1.81\cdot10^{-5}$	$2.22\cdot10^{-5}$	$2.42\cdot10^{-5}$
σ_{Y001}	MPa	919	904	901	895	670	580
n	-	8	8	8	8	8	8
A	$MPa^{-n}s^{-1}$	$1\cdot10^{-42}$	$2.5\cdot10^{-31}$	$8.5\cdot10^{-30}$	$2\cdot10^{-28}$	$6\cdot10^{-27}$	$7\cdot10^{-26}$

In simplified formulation (see Fig. 8) we consider only the sample without equipment, in which zero displacements on the symmetry planes *xz* and *yz* were set, the outer face of the sample parallel to the symmetry plane *xz* was fixed in the direction of the axis *x*. To exclude solid body motions, a number of points on this face were also fixed in the direction of the *y* and zaxes.

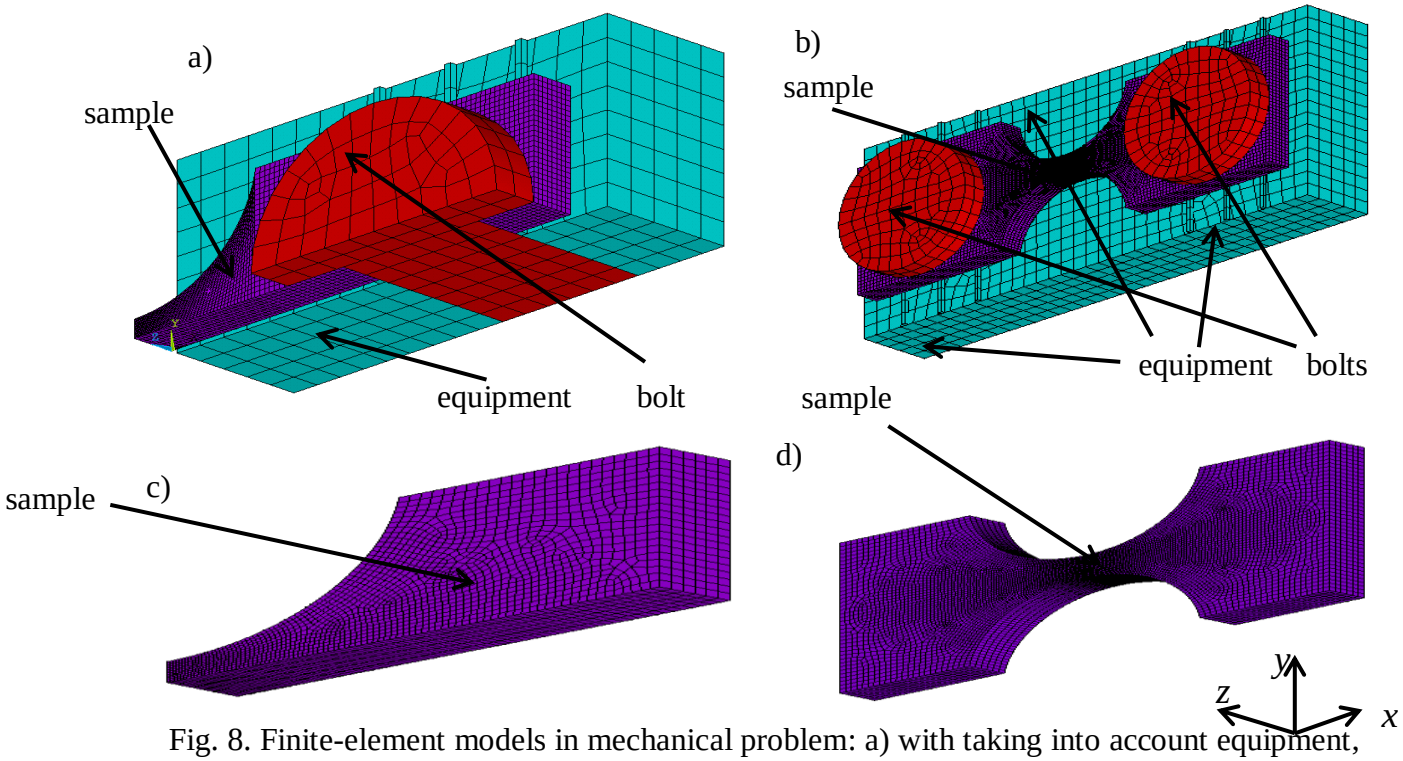

Fig. 8. Finite-element models in mechanical problem: a) with taking into account equipment, symmetric statement, b) with taking into account equipment, full statement, c) without taking into account equipment (simplified formulation), symmetric statement, d) without taking into account equipment (simplified formulation), full statement.

Fig.9 shows distributions of plastic strain intensity for three nickel superalloys and three different temperature modes after 7 cycles (for VZHM4 and VIN3 the length of the sample is 42 mm, for ZHS32 is 50 mm).

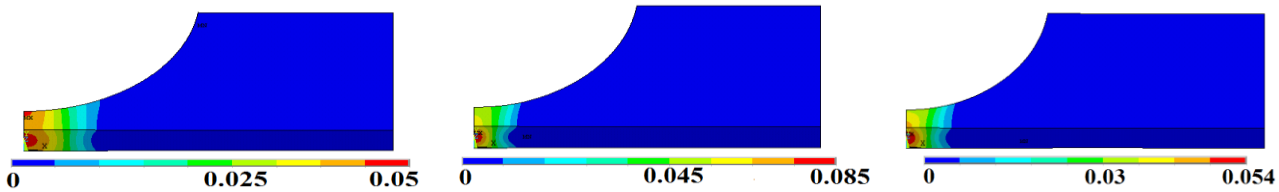

a) b) c)

Fig. 9 Distributions of plastic strain intensity for a) superalloy VZhM4, mode 700÷1050 °C; b) superalloy VIN3, mode 500÷1050 °C; c) superalloy ZhS32, mode 150÷900 °C after 7 cycles

The Table 6 shows the equivalent (effective) length of the sample for the simplified formulation, which has been found from the condition of equality of the inelastic strain ranges with complete model for different alloys. FE simulations showed that effective length doesn't depend on type of hardening (isotropic and kinematic) and doesn't depend on temperature mode. In the FE simulations with acceptable engineering accuracy can be used the value 40 mm. Effective length takes into account the compliance of equipment and its variation in considered range has no appreciable on the results.

Table 6. The equivalent length of the corset sample for different alloys

VZHM4	VIN3	ZHS32
34-42 mm	38-46 mm	40-52 mm

In the FE simulations the length of the specimen for all alloys was taken to be 40 mm.

4. Influence of delay on the thermal fatigue durability and analytical approximation for delay influence

Simulation of inelastic cyclic deformation of corset samples were performed with using of the FE program PANTOCRATOR [15], which allows to apply the micromechanical (physical) models of plasticity and creep for single crystals [16], [17]. The Norton power-type law without hardening was used to describe creep properties. The micromechanical plasticity model accounting 12 octahedral slip systems with lateral and nonlinear kinematic hardening [16] was used in the FE computation for single crystal alloy. FE computations were carried out for a part of a corset sample (simplified FE model with effective length of sample equal 40 mm, see Fig. 9a). The temperature boundary conditions were set from the experimental data at maximum and minimum temperature with linear interpolation in time.

The influence of the delay at maximum temperature on the number of cycles to the formation of macro cracks is analyzed in the range from 1 min to 1 hour for the cyclic loading regimes (see, for example, Fig. 9b) with:

- maximum temperature of 1050 °C and a temperature range of 350 °C and 550 °C;
- maximum temperature of 1100 °C and a temperature range of 900 °;
- maximum temperature of 1000 °C and a temperature range of 750 °;
- maximum temperature of 900 °C and a temperature range of 750 °C.

The heating times in the cycle were 24s, 7s, 18 s, 28s and 17s, the cooling time was 15s, 15s, 40s, 52s and 60s for VZhM4. The heating time in the cycle was 10s, the cooling time was 16s for VIN3. The heating times in the cycle was 35s, 25 s and 15s, the cooling time was 55, 75s and 15s for ZhS32. The mechanical properties for the alloys VZhM4 and VIN3 were taken from the papers [12], [13] and for ZhS32 from [14]. The problem was solved in a quasi-static 3-dimensional formulation. The boundary conditions were zero displacements in the direction of the x-axis on two side faces of the sample with the normal along the x-axis. To exclude solid-state motions, a number of points on these faces in the direction of the y and z axes were also fixed (fig.10).

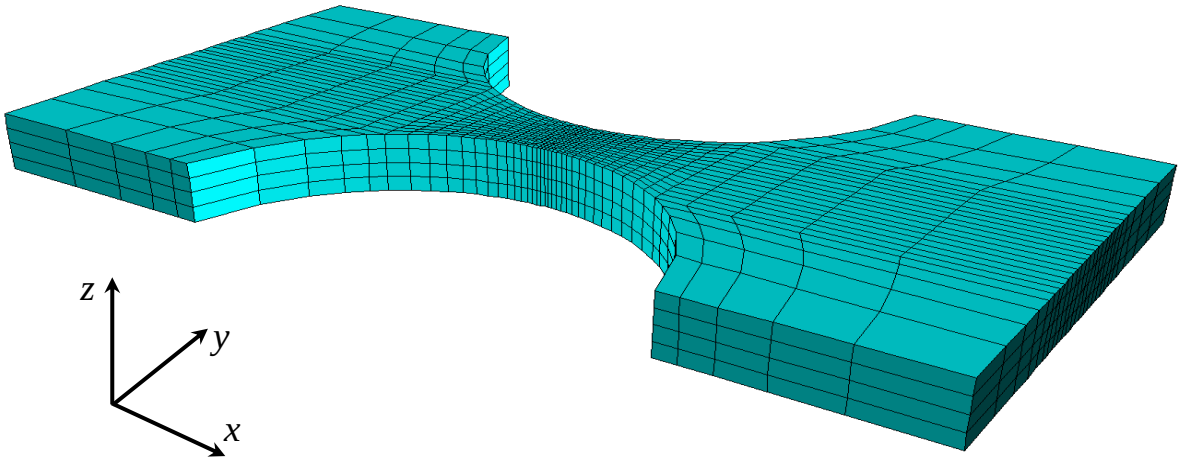

Fig. 10. Finite element model of sample (simplified formulation) for analysis of delay influence

Temperature evolutions in central point of sample with and without delay for temperature modes 700÷1050 °C, 500 ÷1050 °C, 250÷1000 ^{0}C and 150 ÷ 900 °C are presented in fig. 11.

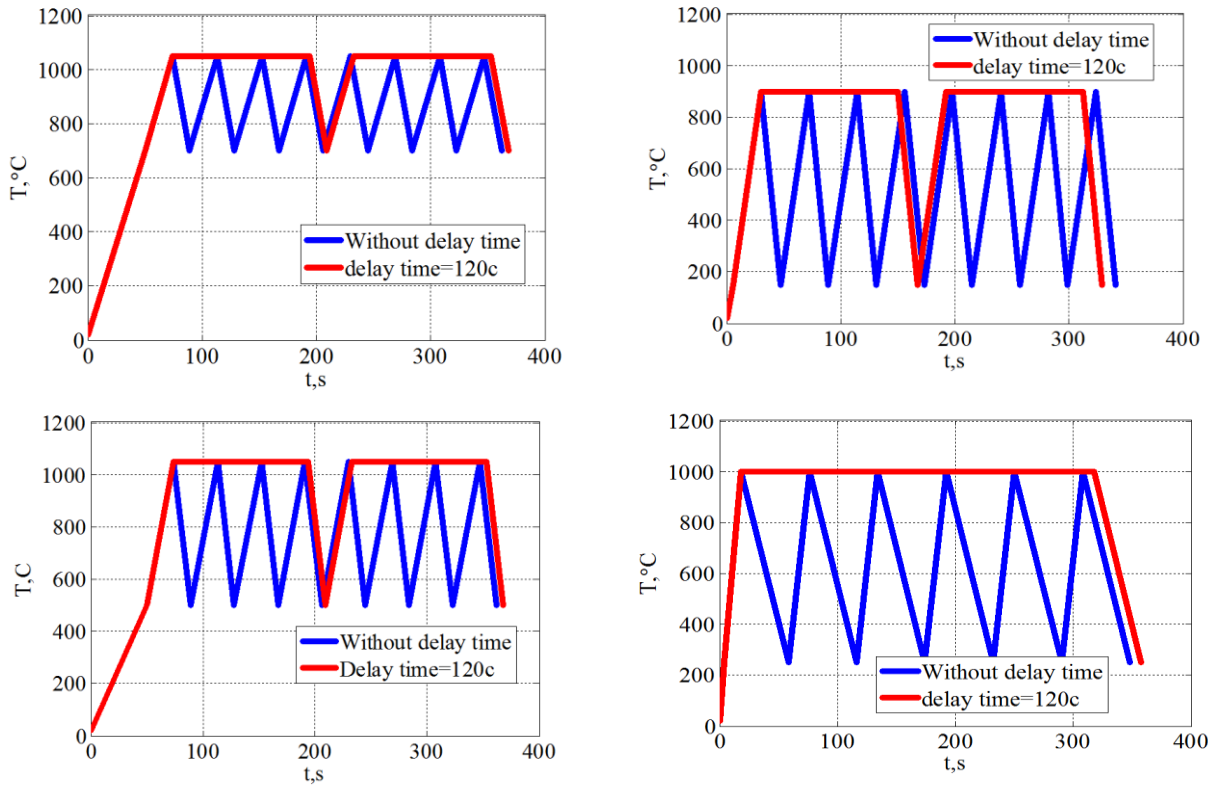

Fig. 11. Temperature evolutions in central point of sample with and without delay for temperature modes 700÷1050 °C, 500 ÷1050 °C, 250÷1000 ^{0}C and 150 ÷ 900 °C.

Damage calculation and estimation of the number of cycles before the formation of macrocracks were made on the basis of deformation four-member criterion [3-5]:

$$D = \sum_{i=1}^{N} \frac{\left(\Delta\varepsilon_{eq_i}^{p}\right)^{k}}{C_1(T)} + \sum_{i=1}^{N} \frac{\left(\Delta\varepsilon_{eq_i}^{c}\right)^{m}}{C_2(T)} + \max_{0\le t\le t_{\max}} \frac{\varepsilon_{eq}^{p}}{\varepsilon_r^{p}(T)} + \max_{0\le t\le t_{\max}} \frac{\varepsilon_{eq}^{c}}{\varepsilon_r^{c}(T)}, \qquad (11)$$

where the first term takes into account the range of plastic strain within the cycle, the second term is the range of creep strain within the cycle, the third term is unilaterally accumulated plastic strain (ratcheting), the fourth term is unilaterally accumulated creep strain. The number of cycles before the formation of macrocracks N is determined from the condition D = 1. The maximum shear strain in the sliding system with normal to the slip plane n and the sliding direction l is considered as equivalent deformation. Usually it takes the values k=2, $m = \frac{5}{4}$, $C_1 = \left(\varepsilon_r^{p}\right)^{k}$, $C_2 = \left(\frac{3}{4}\varepsilon_r^{c}\right)^{m}$, where ε_r^{p} and ε_r^{c} are ultimate strains of plasticity and creep under uniaxial tension. In the FE computations the values of ultimate strain $\varepsilon_r^{p} = \varepsilon_r^{c} = \varepsilon_r = 0.17$ and $\varepsilon_r^{p} = \varepsilon_r^{c} = \varepsilon_r = 0.13$ for VZhM4, $\varepsilon_r^{p} = \varepsilon_r^{c} = \varepsilon_r = 0.18$ and $\varepsilon_r^{p} = \varepsilon_r^{c} = \varepsilon_r = 0.13$ for ZhS32, $\varepsilon_r^{p} = \varepsilon_r^{c} = \varepsilon_r = 0.17$ for VIN3 were used because of dependence ultimate strains from temperature. Improvement of the accuracy of prediction of influence the delay time on durability can be achieved by the refinement of the constant ε_r on the basis of data without delay.

In order to reduce computations, an analytical approximation of delay time influence in thermal fatigue strength was performed. Dependence thermal fatigue strength on delay time was found as

$$N = N_{min} + (N_0 - N_{min}) \cdot e^{-t/50}, \qquad (12)$$

where N is the number of cycles till the formation of macrocracks as function of delay time, N_0 is the the computational number of cycles till the formation of macrocracks in case without delay, N_{min} is the number of cycle in case delat time is equal to 1 hour, t is the delay time. The comparison of the results of FE simulations and experiments concerning the effect of the delay

time at the maximum temperature on the thermal fatigue durability for single-crystal superalloys VZhM4, VIN3 and ZhS32 is given in Fig. 12-13.

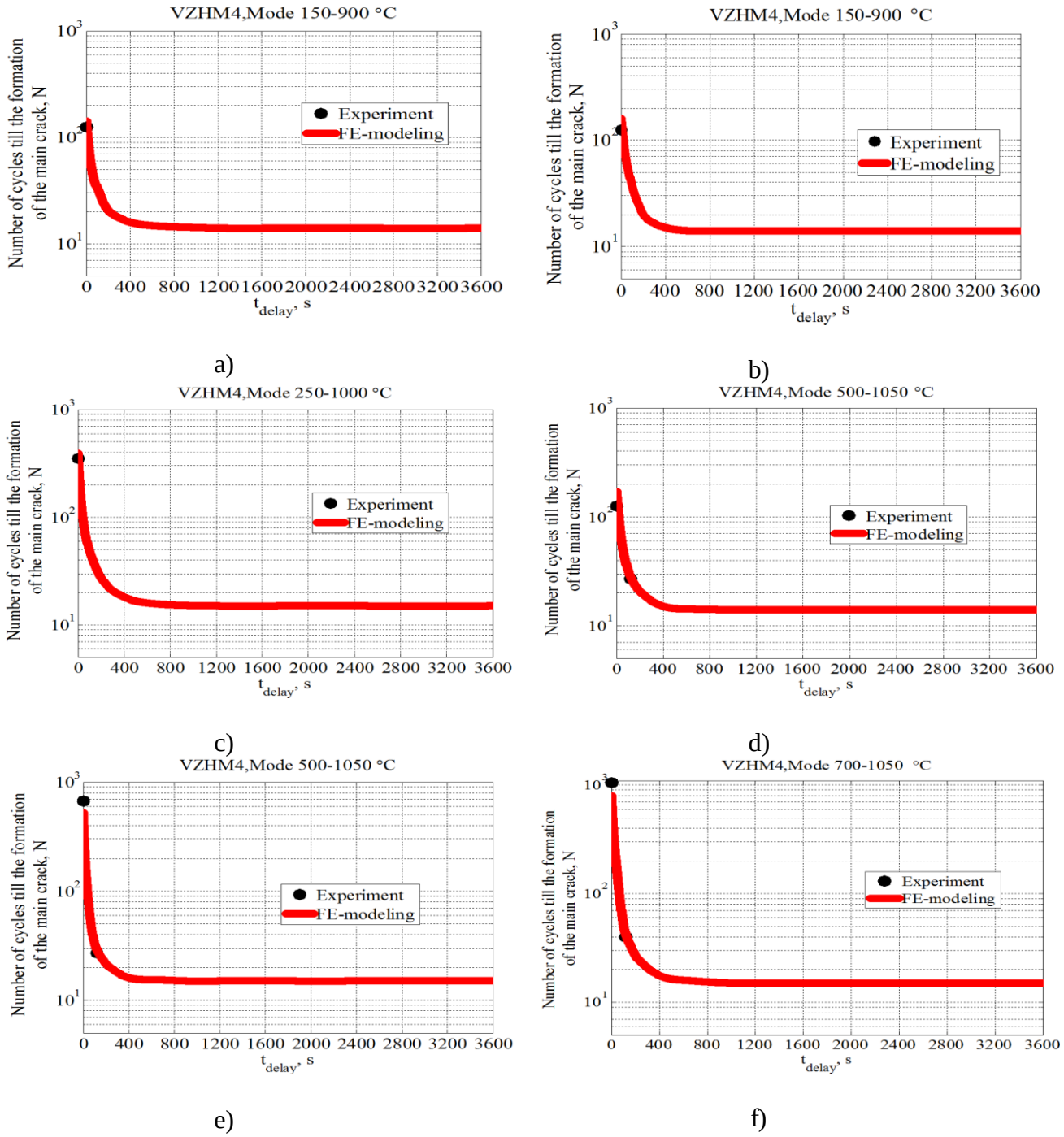

Fig. 12. Comparison of results of FE simulation and experimental data for the alloy VZhM4:
a) mode 150÷900 ^{0}C, heating time is 28s, cooling time is 52s, ε_r= 0.13,
b) mode 150÷900 ^{0}C, heating time is 17s, cooling time is 60s, ε_r= 0.13,
c) mode 250÷1000 ^{0}C, heating time is 18s, cooling time is 40s, ε_r= 0.17,
d) mode 500÷1050 ^{0}C, heating time is 24s, cooling time is 15s, ε_r= 0.17,
e) mode 500÷1050 ^{0}C heating time is 7s, cooling time is 15s, ε_r= 0.17,
f) mode 700÷1050 ^{0}C heating time is 7s, cooling time is 15s, ε_r= 0.17.

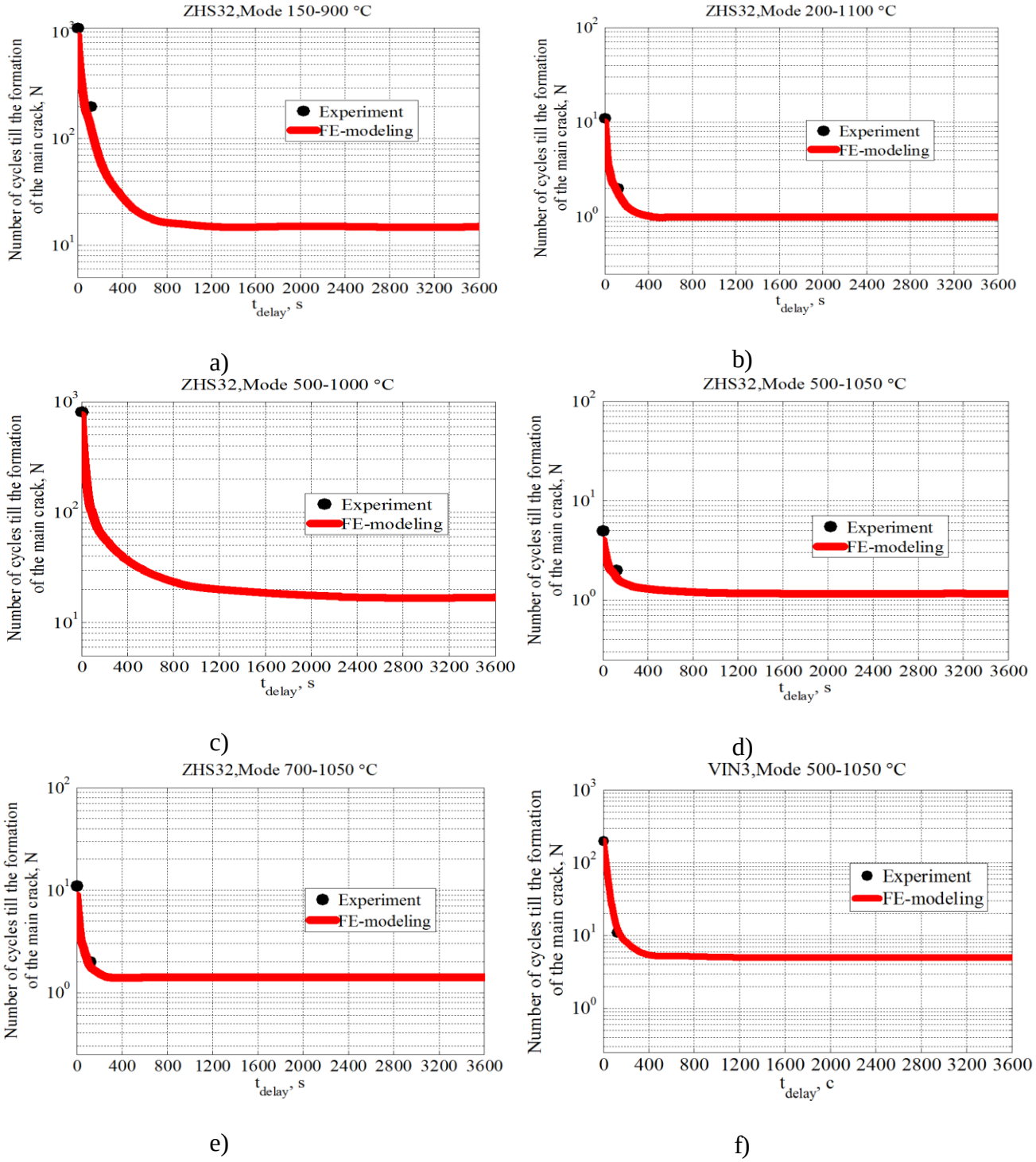

Fig. 13. Comparison of results of FE simulation and experimental data for the alloy:

a) ZhS32, mode 150÷900, heating time is 35 s, cooling time is 55 s, $\varepsilon_r = 0.13$,
b) ZhS32, mode 200÷1100, heating time is 25 s, cooling time is 75 s, $\varepsilon_r = 0.18$,
c) ZhS32, mode 500÷1000, heating time is 10 s, cooling time is 14 s, $\varepsilon_r = 0.18$,
d) ZhS32, mode 500÷1050, heating time is 15 s, cooling time is 15 s, $\varepsilon_r = 0.18$,
e) ZhS32, mode 700÷1050, heating time is 15 s, cooling time is 15 s, $\varepsilon_r = 0.18$
f) VIN3, mode 500÷1050, heating time is 10s, cooling time is 16 s, ε_r = 0.17.

Comparison of results of FE simulation and analytical approximation concerning the effect of the delay time at the maximum temperature on the thermal fatigue durability for single-crystal superalloys VZhM4, VIN3 and ZhS32 is given in Fig. 14-15.

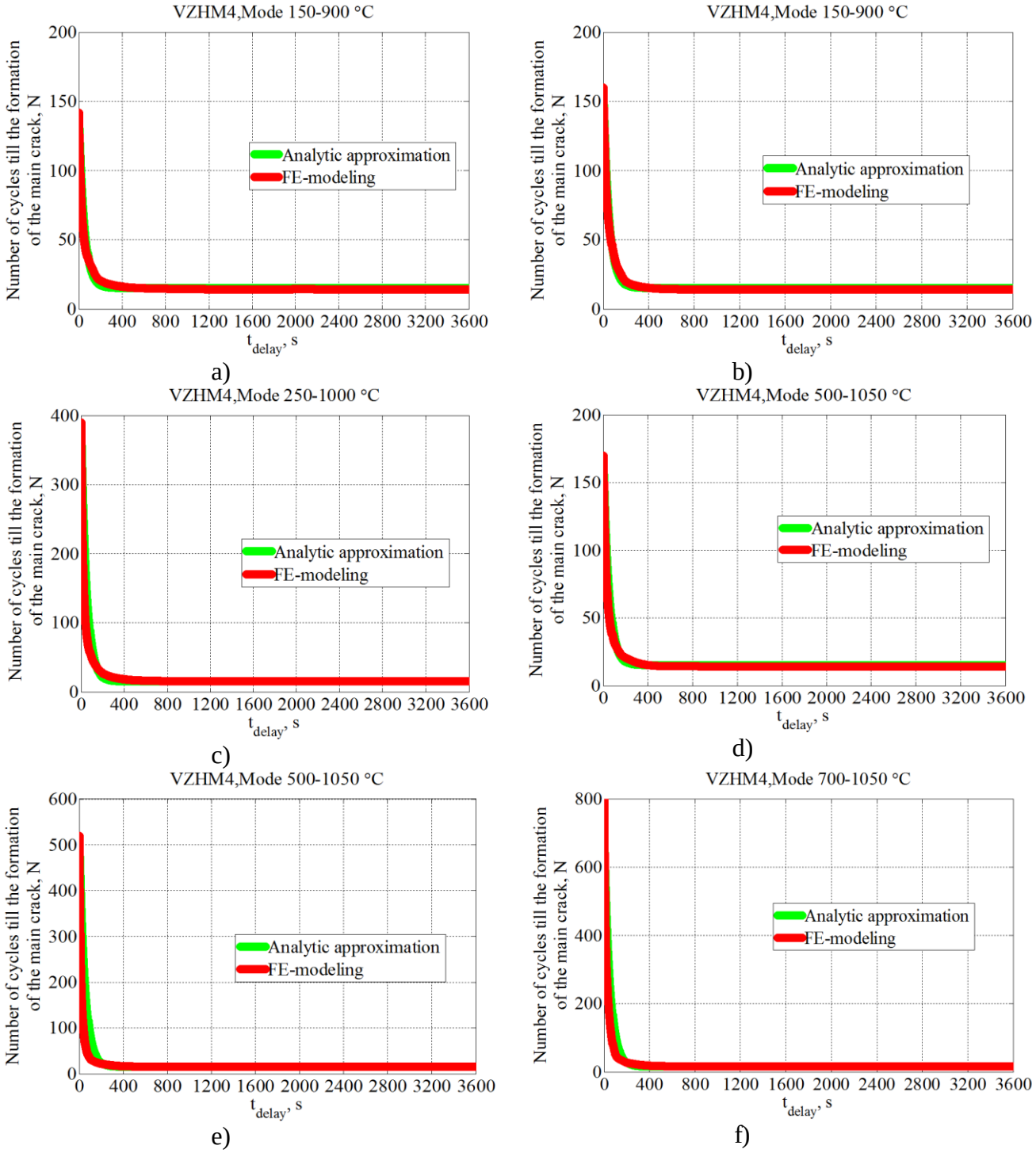

Fig. 14. Comparison of results of FE simulation and analytical approximation for the alloy VZhM4:
a) mode 150÷900 ^{0}C, heating time is 28s, cooling time is 52s,
b) mode 150÷900 ^{0}C, heating time is 17s, cooling time is 60s,
c) mode 250÷1000 ^{0}C, heating time is 18s, cooling time is 40s,
d) mode 500÷1050 ^{0}C, heating time is 24s, cooling time is 15s,
e) mode 500÷1050 ^{0}C heating time is 7s, cooling time is 15s,
f) mode 700÷1050 ^{0}C heating time is 7s, cooling time is 15s.

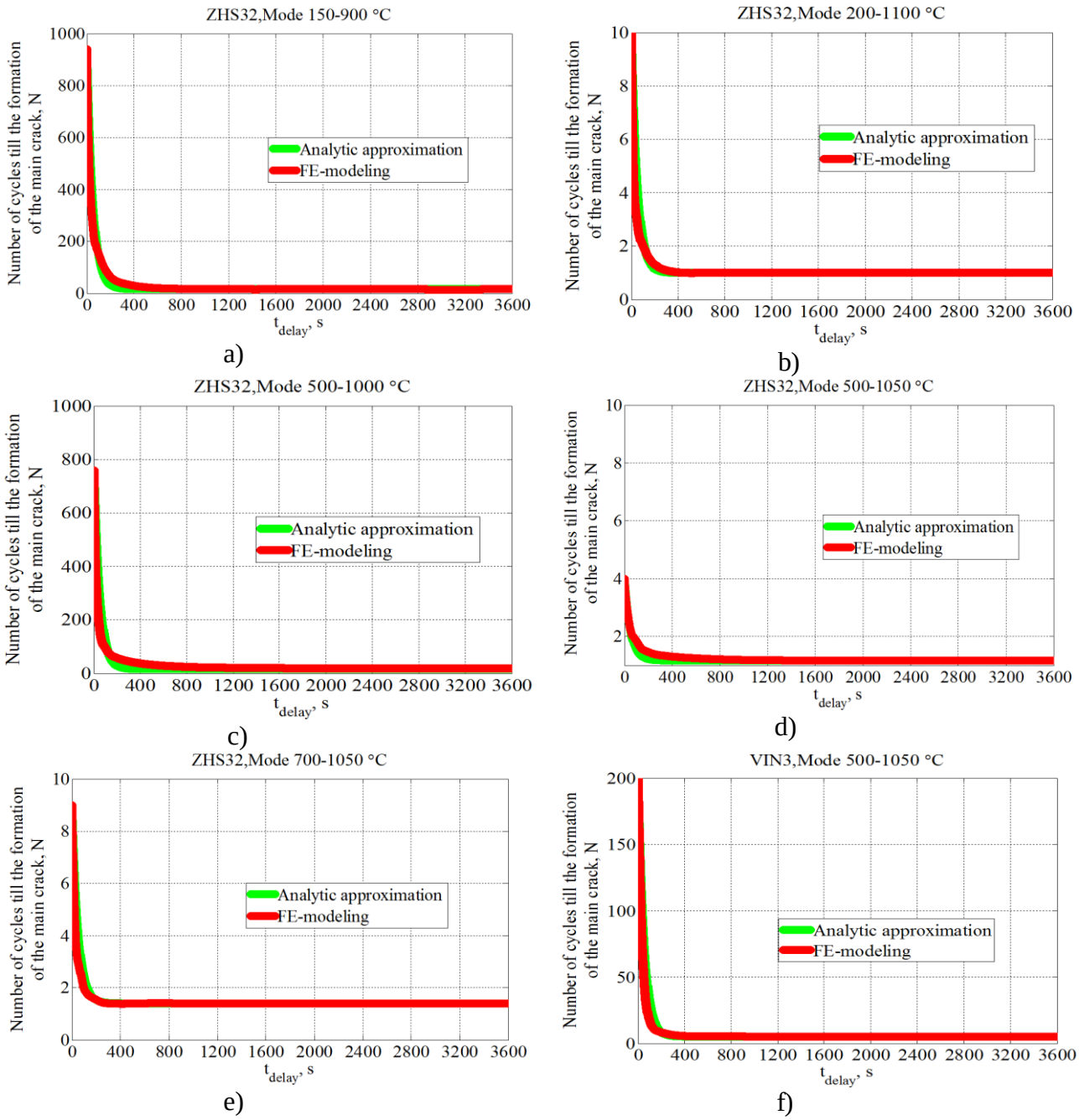

Fig. 15. Comparison of results of FE simulation and analytical approximation for the alloy:
a) ZhS32, mode 150÷900, heating time is 35 s, cooling time is 55 s,
b) ZhS32, mode 200÷1100, heating time is 25 s, cooling time is 75 s,
c) ZhS32, mode 500÷1000, heating time is 10 s, cooling time is 14 s,
d) ZhS32, mode 500÷1050, heating time is 15 s, cooling time is 15 s,
e) ZhS32, mode 700÷1050, heating time is 15 s, cooling time is 15 s,
f) VIN3, mode 500÷1050, heating time is 10s, cooling time is 16 s.

5. Conclusions

The results of the computations and the analytical approximations show a good agreement with the experiment, which suggests that the finite-element computations in combination with application of deformation criterion (3) can be used to predict the thermal-fatigue strength of various single-crystal superalloy samples in wide range temperatures with different delay times.

The research is supported by the SIEMENS Scholarship Program, RFBR grant No. 16-08-00845 and RSF grant No. 18-19-00413.

References

[1] Shalin R.E., Svetlov I.L., Kachanov E.B. and other. Single crystals of nickel heat-resistant alloys-M.: Mashinostroenie, 1997, p.6.

[2] Getsov L.B. Materials and strength of gas turbine parts. - Rybinsk: Turbine technology, 2010. - p. 258-260.

[3] Getsov L.B., Semenov A.S. Criteria of fracture of polycrystalline and single crystal materials under thermal cyclic loading // Proceedings of CKTI. Vol. 296, 2009, p. 83-91.

[4] Semenov A.S., Getsov L.B. Thermal fatigue fracture criteria of single crystal heat-resistant alloys and methods for identification of their parameters // Strength of Materials, 2014. Vol. 46, No. 1, p. 38-48.

[5] Getsov L.B., Semenov A.S., Staroselsky A. A failure criterion for single-crystal superalloys during thermocyclic loading // Materials and technology. 2008. Vol. 42, p. 3–12.

[6] Petrushin N.O. Logunov A.V., Kovalev A.I., Zverev A. F., Toropov V. M., Fedotov N. H. Thermophysical properties of Ni3Al-Ni3Nb directly crystallized eutectic composition // High temperature thermophysics, 1976,Vol.14, № 3,p. 649-652.

[7] Zinoviev V.E., Thermo-physical properties of metals at high temperatures. Moscow: Metallurgia, 1989, p.324.

[8] Chirkin V.S. Thermophysical properties of nuclear materials. Moscow:Atomizdat, 1968, p. 161.

[9] Maslenkov S.B., Maslenkova E.A. Steels and alloys for high temperatures. Moskow: Metallurgia, 1991, p.150.

[10] Курант Р., Гильберт Д. Методы математической физики. Том 2. Пер. с нем. - М.-Л.: ГТТИ, 1945. — 620 с.

[11] May S., Semenov A.S. Modeling of inelastic cyclic deformation of monocrystalline specimens // Proc. of the XXXIX week of science of SPbGPU. 2010. Vol. 5. P. 73-74.

[12] Kablov E.N., Petrushin N.O., Svetlov I.L., Demonis I.M. Nickel casting heat-resistant alloys of the new generation. The jubilee nauch.- tech. sat. Aviation materials and technologies. M: Proceedings of VIAM. 2012, p. 36-52.

[13] Semenov S.G., Getsov L.B., Semenov A.S., Petrushin N.V., Ospennikova O.G., Zhivushkin A.A. The issue of enhancing resource capabilities of nozzle blades of gas turbine engines through the use of new single crystal alloy // Journal of Machinery Manufacture and Reliability. 2016. No.4, p. 30-38.

[14] Getsov L.B., Semenov A.S., Tikhomirova E.A., Rybnikov A.I. Thermocyclic and static failure criteria for single crystal superalloys of gas turbine blades // Materials and technology.2014. No.2, p.255-260.

[15] Semenov A.S. PANTOCRATOR–finite-element program specialized on the solution of non-linear problems of solid body mechanics/ Proc. of the V-th International. Conf. "Scientific and engineering problems of reliability and service life of structures and methods of their decision". SPb.: Izd-vo SPbSPU, 2003. p. 466-480.

[16] Cailletaud G.A. Micromechanical approach to inelastic behaviour of metals // Int. J. Plast., 1991, 8, p. 55-73.

[17] Semenov A.S. Identification of anisotropy parameters of phenomenological plasticity criterion for single crystals on the basis of micromechanical model // Scientific and technical sheets SPbGPU. Physical and mathematical Sciences. 2014. No. 2 (194). p. 15-29.

[18] http://www.ipme.ru/e-journals/MPM/